Kondo effect under the influence of spin-orbit coupling in a quantum wire

V. Lopes[1,2], G. B. Martins[3], M. Manya[4], E. V. Anda[1]

Kondo effect under the influence of spin-orbit coupling in a quantum wire

[1] Departamento de Física, Pontifícia Universidade Católica do Rio de Janeiro (PUC-Rio), Rio de Janeiro, Rio de Janeiro, 22453-900, Brazil
[2] Departamento de Física Aplicada, Universidad de Alicante, San Vicente del Raspeig, 03690, Alicante, Spain
[3] Instituto de Física, Universidade Federal de Uberlândia, Uberlândia, Minas Gerais, 38400-902, Brazil
[4] Instituto de Física, Universidade Federal Fluminense, 24210-346 Niterói, RJ, Brazil

E-mail: gbmartins@ufu.br

E-mail: enriquevictoranda@gmail.com

Abstract. The analysis of the impact of spin-orbit coupling (SOC) on the Kondo state has generated considerable controversy, mainly regarding the dependence of the Kondo temperature T_K on SOC strength. Here, we study the one-dimensional (1D) single impurity Anderson model (SIAM) subjected to Rashba (α) and Dresselhaus (β) SOC. It is shown that, due to time-reversal symmetry, the hybridization function between impurity and quantum wire is diagonal and spin independent (as it is the case for the zero-SOC SIAM), thus the finite-SOC SIAM has a Kondo ground state similar to that for the zero-SOC SIAM. This similarity allows the use of the Haldane expression for T_K, with parameters renormalized by SOC, which are calculated through a physically motivated change of basis. Analytic results for the parameters of the SOC-renormalized Haldane expression are obtained, facilitating the analysis of the SOC effect over T_K. It is found that SOC acting in the quantum wire exponentially decreases T_K while SOC at the impurity exponentially increases it. These analytical results are fully supported by calculations using the Numerical Renormalization Group (NRG), applied to the wide-band regime, and the Projector Operator Approach, applied to the infinite-U regime. Literature results, using Quantum Monte Carlo, for a system with Fermi energy near the bottom of the band, are qualitatively reproduced, using NRG. In addition, it is shown that the 1D SOC SIAM for arbitrary α and β displays a persistent spin helix SU(2) symmetry similar to the one for a 2D Fermi sea with the restriction $\alpha = \beta$.

PACS numbers:

Submitted to: *J. Phys.: Condens. Matter*

1. Introduction

It is well-known that magnetic impurities, when diluted in small concentrations in a metallic host, impart singular characteristics to its properties, most notably its resistivity, which acquires a minimum as a function of temperature [1]. This phenomenon, first observed in the mid 1930s [2], was given a satisfactory explanation only in 1964 by Jun Kondo [3]: the localized magnetic moment of the impurity is screened by the spins of the conduction electrons below a characteristic temperature, the so-called Kondo temperature T_K.

Recently, there has been much interest in the study of the Kondo regime of a magnetic impurity coupled to a metallic substrate presenting SOC. Theoretical work by Meir and Wingreen in 1994 [4] concluded that SOC does not suppress the Kondo effect. This subject lay dormant for many years, until a surge in interest (see Refs. 5, 6) was stimulated by SOC's importance for systems with spintronic applications, e.g., the Datta-Das spin transistor [7]. Thus, SOC's effect on the Kondo state of a magnetic impurity, or a quantum dot, embedded in a two-dimensional (2D) system has received, in the last decade, renewed attention [8–13]. However, less attention has been given to an impurity coupled to a one-dimensional (1D) system [14, 15]. Nevertheless, for either 1D or 2D, the effect SOC has on the Kondo regime became a controversial topic. Indeed, while some theory [15] and experimental [16] groups argue that SOC suppresses the Kondo effect, other groups arrived at the opposite conclusion, arguing that SOC enhances T_K [10, 12, 14]. Other studies predict that T_K is not affected by SOC [4, 8], while still others concluded that the effect depends upon the parameters defining the system [9]. It is expected that in a 1D conductor, where SOC produces only forward and backward scattering, it should have a stronger influence than in 2D systems [14]. On one hand, Sousa *et al.* have concluded, using a renormalization group analysis, that SOC exponentially increases T_K in 1D [14]. On the other hand, using the Hirsch-Fye Quantum Monte Carlo simulation and a slave-boson mean-field approximation, Chen and Han concluded that T_K is reduced by SOC [15].

Here, we open a short parenthesis to mention that a related phenomenon, viz., Kondo effect in topological insulators (TI), bears some resemblances to the Kondo effect discussed here, but the list of differences—e.g., in TI we have absence of spin precession, no interband scattering, energy dependent density of states, etc. (see Ref. [17])—is too large to warrant a direct comparison to our results.

The discussion above implies that the physics associated to the Kondo state under the effect of SOC requires a more profound understanding, comprising an effort of synthesis and clarification. Finally, most of the studies considered just SOC acting in the bulk, neglecting SOC acting at the impurity itself [18].

In this work, we show that the Haldane expression for T_K [1, 19, 20], originally obtained for a zero-SOC single impurity Anderson model (SIAM), is still valid, with

renormalized parameters, for a SIAM in which the Fermi sea, modeled as a 1D quantum wire (QW) has Rashba [21] and linear Dresselhaus [22] SOC, with couplings α and β, respectively. This occurs because the hybridization matrix, which incorporates the coupling between impurity and Fermi sea, and thus determines the Kondo state, is diagonal and spin independent (thus a scalar function) for both finite- and zero-SOC models. This may seem surprising, as SOC breaks full spin SU(2) symmetry. However, we argue that this property of the hybridization function is guaranteed, in our case, by time-reversal symmetry, which is preserved by SOC. To illustrate that, and to find analytical expressions for the renormalized parameters of the Haldane expression for T_K, we perform a change of basis that places the finite-SOC SIAM Hamiltonian into a form similar to that of the zero-SOC SIAM. This basis is then used to define a global pseudo-spin [23] wave-vector-dependent operator, obeying an SU(2) algebra, whose components (denoted by $\boldsymbol{S}_Q^i$) commute with the finite-SOC SIAM Hamiltonian for arbitrary values of α and β. This shows that the Hamiltonian has a pseudo-spin SU(2) symmetry, similar in spirit to the persistent spin helix (PSH) SU(2) symmetry found by Bernevig *et al.* [24] for a 2D model, with the restriction $\alpha = \beta$.

We then present numerical support to the analytical results described above by using the Numerical Renormalization Group (NRG) in two different regimes of the SIAM: (i) a wide-band regime, i.e., where the half band-width D is much larger than the impurity Coulomb repulsion U and its coupling to the band Δ. In that case, the analytical results obtained through the appropriate Haldane expression for the Kondo temperature [see Eq. [37] in Ref. 19, reproduced below as Eq. (11)], are in excellent agreement with the NRG results, showing that, indeed, in this regime, SOC exponentially decreases the Kondo temperature; (ii) in an intermediate regime, where $U = D > \Delta$, with the Fermi energy close to the bottom of the band. The motivation for analyzing this regime is to compare the results obtained by Chen and Han [15], using Quantum Monte Carlo (QMC) calculations, with our NRG results. Finally, the analytical results for the Kondo temperature are compared to numerical results obtained by the Projector Operator Approach [25, 26] (POA), for yet a third regime, that of infinite Coulomb repulsion, and shown to be in excellent agreement.

2. Model

The system consists of a quantum wire (QW), i.e., a 1D Fermi sea (along the x-axis), coupled to a magnetic impurity. It is modeled by a SIAM [1, 27] extension, modified to include Rashba [21] and linear Dresselhaus [22] SOC. The Hamiltonian is given by $H = H_{wire} + H_{imp} + H_{hyb}$, where

$$\begin{aligned} H_{wire} = &- \sum_{k,\sigma} \left(2t\cos k - \mu\right) c_{k\sigma}^{\dagger} c_{k\sigma} \\ &- \sum_{k} 2\sin k \left(\gamma c_{k\uparrow}^{\dagger} c_{k\downarrow} + h.c.\right), \end{aligned} \tag{1}$$

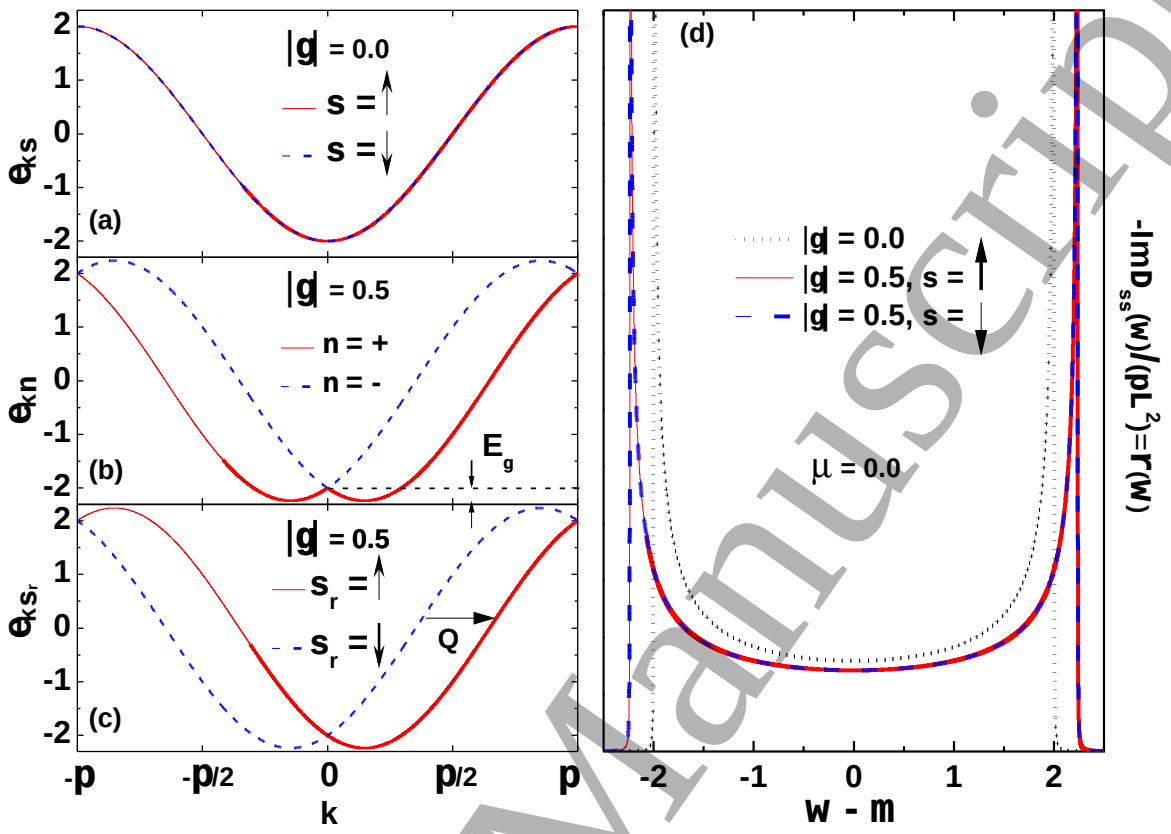

Figure 1. (a) Quantum wire dispersion $\epsilon_{k\sigma}+\mu$ for zero-SOC. Solid/dashed (red/blue) curve for $\sigma =\uparrow / \downarrow$ (b) Dispersion $\epsilon_{k\nu}$ for $|\gamma| = 0.5$. Here, the bands are characterized by the helicity quantum number ν: solid/dashed (red/blue) curve for $\nu = +/-$ (c) Same as in (b), but now the bands are characterized by the quantum number σ_r: solid/dashed (red/blue) curve for $\sigma_r =\uparrow / \downarrow$. Wave vector Q, connecting both bands, is discussed in the text. (d) DOS $\rho(\omega) = -\mathrm{Im}\Delta_{\sigma\sigma}(\omega)/\left(\pi\Lambda^2\right)$ with and without SOC. The dotted black curve corresponds to zero-SOC ($|\gamma| = 0$) and the solid/dashed (red/blue) curves correspond to $|\gamma| = 0.5$, for $\sigma =\uparrow / \downarrow$, for an arbitrary spin quantization axis. Note in panel (b) the definition of the SOC energy, E_γ, used in Fig. 3(a). All results are shown for $\mu = 0$.

$$H_{imp} = \sum_{\sigma} \epsilon_0 n_{0\sigma} + \sum_{\sigma} \frac{U}{2} n_{0\sigma} n_{0\bar{\sigma}}, \tag{2}$$

$$H_{hyb} = \sum_{k} \Bigg[\sum_{\sigma} \left(V_k c^{\dagger}_{k\sigma} c_{0\sigma} \right) + i\gamma_{imp,k} c^{\dagger}_{k\downarrow} c_{0\uparrow} + i\gamma^{*}_{imp,k} c^{\dagger}_{k\uparrow} c_{0\downarrow} + h.c. \Bigg]. \tag{3}$$

In the equations above, $c^{\dagger}_{k\sigma}$ ($c_{k\sigma}$) creates (annihilates) an electron with momentum k and spin σ in the QW, which is modeled by a 1D tight-binding approximation with nearest-neighbor hopping t, lattice parameter $a = 1$, and $\mu = \epsilon_F$ is the chemical potential (Fermi energy). Note that μ will be set to 0 (half-filling) for most calculations, except

when we investigate the Kondo state for a Fermi energy close to the bottom of the band, when it will be set to $\mu = \epsilon_F = -0.8$. The second term in Eq. (1) describes the SOC [28], where $\gamma = \beta + i\alpha$, $i = \sqrt{-1}$. The impurity is modeled by H_{imp}, Eq. (2), where ϵ_0 is the impurity orbital energy and U is the Coulomb repulsion for its double occupancy. The operator $c^\dagger_{0\sigma}$ ($c_{0\sigma}$) creates (annihilates) an electron with spin σ at the impurity, and $n_{0\sigma} = c^\dagger_{0\sigma} c_{0\sigma}$. Equation (3) represents the coupling between the impurity and the QW, where the first term denotes the hybridization V_k, which preserves the electron spin between the impurity and the QW, while the other term represents the spin-flip coupling due to the local SOC at the impurity, of magnitude $\gamma_{imp,k}$ [18, 29]. As it is the case for the hybridization V_k, $\gamma_{imp,k}$ depends, in principle, upon the linear momentum k. However, for simplicity, we will assume that the two parameters are k-independent, denoted from now on as V and γ_{imp}. Note that, in the literature, a linear approximation of the electronic dispersion, valid for small values of k [14, 15], is frequently used. In the present study, we will not make this approximation, taking k in the whole interval, i.e., $-\pi \leq k \leq \pi$. Finally, we note that the results shown in Figs. 1 and 4 were obtained for $t = 1$ as the energy unit, while for the NRG results in Figs. 2 and 3 the half band-width $D = 1$ was used as energy unit (thus, $t = 1/2$).

3. Spin rotation and SIAM Hamiltonian in the σ_r basis

Let us first analyze the decoupled (no impurity) QW. In Fig. 1(a), it is shown the dispersion when there is no SOC, $\gamma = 0$ (solid/dashed (red/blue) curve for spin up/down). In this case, the Hamiltonian has spin SU(2) symmetry, i.e., the spin is a good quantum number and the energy dispersion does not depend upon it. Thus, the eigenstates $|k\uparrow\rangle$ and $|k\downarrow\rangle$ (in the S_z basis) are degenerate and the z-axis can be chosen to point in any direction. However, for finite-SOC, the spin angular momentum, for an arbitrary quantization axis, is no longer a good quantum number, because of the spin-mixing term in Eq. (1). Nonetheless, as SOC preserves time-reversal symmetry, we can define a helicity operator h such that $[h, H_{wire}] = 0$, and whose eigenvalues $\nu = \pm$ are thus good quantum numbers for the eigenstates of H_{wire}. Indeed, in the helicity basis

$$c^\dagger_{k\nu} = \frac{1}{\sqrt{2}} \left(c^\dagger_{k\uparrow} + \nu s_k e^{i\phi} c^\dagger_{k\downarrow} \right), \tag{4}$$

where $\phi = \tan^{-1}(\alpha/\beta)$ and $s_k = \mathrm{sgn}(k)$, $H_{wire} = \sum_{k,\nu} \epsilon_{k\nu} c^\dagger_{k\nu} c_{k\nu}$ is diagonal, with a dispersion relation

$$\epsilon_{k\nu} = -2t \cos k - 2\nu|\gamma||\sin k| + \mu. \tag{5}$$

Figure 1(b) shows $\epsilon_{k\nu}$, for $|\gamma| = 0.5$, plotted as a function of k for each ν: the lower band (solid (red) curve) associated to the quantum number $\nu = +$ and the upper band (dashed (blue) curve) to $\nu = -$. As SOC preserves time-reversal symmetry, i.e., $[\Theta, H_{wire}] = 0$, where Θ is the time-reversal operator, we have degenerate Kramers doublets [30] in the same helicity band, $\epsilon_{k\nu} = \epsilon_{-k\nu}$.

However, as the helicity ν is not defined for the impurity, its coupling to the QW mixes helicity channels and ν is not longer a good quantum number. We can rewrite $H_{wire} + H_{hyb}$ in a more convenient form by choosing another basis. The key here is to realize that the $|k\nu\rangle = c^\dagger_{k\nu}|0\rangle$ are eigenstates of the S_r component of the spin angular momentum pointing along the direction $\hat{\boldsymbol{r}} \equiv [\theta = \pi/2, \phi]$, for $s_k = +$, and along the opposite direction $-\hat{\boldsymbol{r}} \equiv [\theta = \pi/2, \phi + \pi]$, for $s_k = -$. Thus, $\hat{\boldsymbol{r}}$ determines the direction of what is conventionally called the effective "spin-orbit magnetic field" [31], i.e., $\boldsymbol{B}^{\text{eff}}_{\text{SOC}}(k) = |\gamma| \sin(k)\, \hat{\boldsymbol{r}}$ [see Eq. (5)], such that when k changes to $-k$ the effective magnetic field points in the opposite direction, thus conserving time-reversal symmetry. Note that, in this context, 'up' and 'down' refers to spin quantization 'along $\hat{\boldsymbol{r}}$', where $\hat{\boldsymbol{r}}$ lays on the xy plane, somewhere in its first quadrant, depending on the ratio α/β. Thus, as we will see next, for finite SOC, the presence of the impurity will make it advantageous to work in the S_r basis, with spin quantum number σ_r.

The ground state of the Kondo regime is a singlet formed between the impurity and the conduction electrons, whose spins in the finite-SOC QW are good quantum numbers when quantized along the $\hat{\boldsymbol{r}}$ direction. As a consequence, it is natural to expect that it will be advantageous to choose a quantization axis along $\hat{\boldsymbol{r}}$ for the impurity as well. Thus, if we take $\hat{\boldsymbol{r}} \equiv [\theta = \pi/2, \phi]$ as the spin quantization axis for the impurity, then the spin up ($\sigma_r = \uparrow \equiv +$) and spin down ($\sigma_r = \downarrow \equiv -$) impurity states are given by $c^\dagger_{0\sigma_r} = 1/\sqrt{2}(c^\dagger_{0\uparrow} + \sigma_r e^{i\phi} c^\dagger_{0\downarrow})$, where $c^\dagger_{0\sigma_r}(c_{0\sigma_r})$ creates (annihilates) an electron at the impurity with spin σ_r, quantized along the $\hat{\boldsymbol{r}}$ direction, with the understanding that when σ_r appears as a subscript it means $(\uparrow, \downarrow)$, and when it appears in an equation it means $(+, -)$, respectively.

The total Hamiltonian in this new basis is written as

$$H = \sum_{k,\sigma_r} \epsilon_{k\sigma_r} c^\dagger_{k\sigma_r} c_{k\sigma_r} + \sum_{\sigma_r} \epsilon_0 n_{0\sigma_r} + \sum_{\sigma_r} \frac{U}{2} n_{0\sigma_r} n_{0\bar{\sigma}_r} + \sum_{k,\sigma_r} \Lambda \left(c^\dagger_{k\sigma_r} c_{0\sigma_r} + c^\dagger_{0\sigma_r} c_{k\sigma_r} \right), \tag{6}$$

where $n_{0\sigma_r} = c^\dagger_{0\sigma_r} c_{0\sigma_r}$ is the impurity number operator, $c^\dagger_{k\sigma_r}(c_{k\sigma_r})$ creates (annihilates) an electron at the Fermi sea with momentum k and spin σ_r and $\Lambda = (V^2 + |\gamma_{imp}|^2)^{1/2}$, with a dispersion

$$\epsilon_{k\sigma_r} = -2\sqrt{t^2 + |\gamma|^2} \cos(k - \sigma_r \varphi) + \mu, \tag{7}$$

where $\varphi = \tan^{-1}(|\gamma|/t)$. Each one of the bands in $\epsilon_{k\sigma_r}$, displaced from each other along the k-axis by $Q = 2\varphi$, is associated to one of the S_r eigenvalues $\sigma_r = \uparrow, \downarrow$, as shown in Fig. 1(c).

4. Time-reversal and the Hybridization Function

It is well known that the hybridization function (which determines the properties of the Kondo state [32]) for the zero-SOC SIAM is a spin-independent scalar function,

denoted by $\Delta(\omega)$. As the Hamiltonian shown in Eq. (6) is similar to that for the zero-SOC SIAM, one may be led to assume that this is still the case for the finite-SOC hybridization function. However, there is an important detail in Eq. (6): the QW dispersion $\epsilon_{k\sigma_r}$ *is* spin dependent [see Eq. (7) and Fig. 1(c)], which may imply that the hybridization function is spin dependent. A simple numerical calculation shows that this is not the case [see Fig. 1(d)]. A general argument shows that time-reversal symmetry requires the finite-SOC SIAM hybridization matrix $\tilde{\Delta}_{\sigma\sigma'}(\omega)$ to be diagonal and spin-independent for any spin orientation σ along an arbitrary quantization axis, like the one for the zero-SOC SIAM [32]. Indeed, the matrix elements of the 2×2 hybridization matrix can be written as $\tilde{\Delta}_{\sigma\sigma'}(\omega) = \sum_k \Sigma_{\sigma\sigma'}(k,\omega)$, where $\Sigma_{\sigma\sigma'}(k,\omega) = \Lambda^2 G^{wire}_{\sigma\sigma'}(k,\omega)$, and $G^{wire}_{\sigma\sigma'}(k,\omega)$ is the single-particle Green's function for the QW. An analysis of the expressions for the matrix elements $\Sigma_{\sigma\sigma'}(k,\omega)$ indicates that their parity, in relation to k, can be readily obtained from Eq. (1): no-spin-flip terms $\Sigma_{\sigma\sigma}(k,\omega)$, produced by the first term in H_{wire}, which is associated to the kinetic energy $p^2/2m$, are therefore even in k and spin independent, while non-diagonal spin-flip terms $\Sigma_{\sigma\bar{\sigma}}(k,\omega)$ are produced by the (SOC) second term in H_{wire}, which, *to preserve time-reversal symmetry*, has to be odd in k. Thus, integrating $\Sigma_{\sigma\sigma'}(k,\omega)$ in k to obtain $\tilde{\Delta}_{\sigma\sigma'}(\omega)$ results in $\tilde{\Delta}_{\uparrow\uparrow}(\omega) = \tilde{\Delta}_{\downarrow\downarrow}(\omega) = \tilde{\Delta}(\omega)$ and $\tilde{\Delta}_{\uparrow\downarrow}(\omega) = \tilde{\Delta}_{\downarrow\uparrow}(\omega) = 0$. Therefore, as previously advertised, the spin independence of the hybridization function for the finite-SOC SIAM (despite the broken spin SU(2) symmetry) is guaranteed by the time-reversal symmetry. To illustrate these results, $-\mathrm{Im}\Delta_{\sigma\sigma}(\omega)/(\pi\Lambda^2) = \rho(\omega)$ is plotted in Fig. 1(d) for finite-SOC (solid/dashed (red/blue) curve for an arbitrary spin orientation $\sigma = \uparrow / \downarrow$), and, as expected, it does not depend upon the spin orientation.

5. Pseudo-spin SU(2) Symmetry

Motivated by the fact that the dispersion relation in Eq. (7) satisfies the identity $\epsilon_{k\sigma_r} = \epsilon_{k+Q\bar{\sigma}_r}$, which guarantees that a 2D Fermi sea has a pseudo-spin SU(2) symmetry (when $\alpha = \beta$) [24], we analyze if this is the case too for our system. To accomplish that, we generalize the problem to treat the Anderson model by introducing the spinor operators (in the σ_r basis) $\boldsymbol{c}^\dagger_{kQ} = \{c^\dagger_{k\uparrow} \;\; c^\dagger_{k+Q\downarrow}\}$ and $\boldsymbol{c}^\dagger_0 = \{c^\dagger_{0\uparrow} \;\; c^\dagger_{0\downarrow}\}$, and with them construct the operators $2\boldsymbol{S}^i_Q = \sum_k \boldsymbol{c}^\dagger_{kQ}\boldsymbol{\sigma}^i\boldsymbol{c}_{kQ} + \boldsymbol{c}^\dagger_0\boldsymbol{\sigma}^i\boldsymbol{c}_0$, where the $\boldsymbol{\sigma}^i$ are the Pauli matrices and $Q = 2\varphi$ [see Eq. (7)]. These operators obey the angular momentum commutation relations $[\boldsymbol{S}^i_Q, \boldsymbol{S}^j_Q] = i\varepsilon^{ijl}\boldsymbol{S}^l_Q$, where ε^{ijl} is the Levi-Civita symbol. It can be shown that the $\boldsymbol{S}^i_Q$ (for $i = x, y, z$) commute with the finite-SOC SIAM Hamiltonian. Note that, as in Ref. [24], the commutation $[\boldsymbol{S}^i_Q, H] = 0$ is satisfied because of the equality $\epsilon_{k+Q\sigma_r} = \epsilon_{k\bar{\sigma}_r}$, when $Q = 2\varphi$ [see Eq. (7) and Fig. 1(c)] showing that our Hamiltonian is pseudo-spin SU(2) symmetric. Thus, the operators $\boldsymbol{S}^i_Q$ are the generators of the symmetry operations connected to the PSH states [24], which the authors believe may be associated with the structure of the Kondo cloud formed in our system, as observed in a previous work on Topological Insulators (see Fig. 10(a) in Ref. [33]).

6. Renormalized Haldane Expression

Through the application of Anderson's poor man's scaling approach [34] to the SIAM, different expressions for the Kondo temperature T_K can be found for a variety of parameter regimes [1]. All of them, collectively known as Haldane expression [19, 20], are proportional to an exponential $\exp\left(\pi\epsilon_0(\epsilon_0+U)/2\Delta U\right)$ multiplied by a function of Δ, D, ϵ_0 and U, whose form depends on these parameters relative values. In the wide-band limit, i.e., $D \gg U, \Delta, |\epsilon_0|$, Haldane obtained (see Eq. [37] in Ref. 19)

$$T_K = 0.364\left(2\Delta U/\pi\right)^{\frac{1}{2}} \exp\left[\frac{\epsilon_0\left(\epsilon_0+U\right)}{2\Delta U/\pi}\right], \tag{8}$$

where $\Delta = \pi V^2 \rho\left(\epsilon_F\right)$ and $\rho\left(\epsilon_F\right)$ is the band DOS at the Fermi energy ϵ_F. As our Hamiltonian [Eq. (6)] is formally equivalent to the zero-SOC SIAM Hamiltonian used to obtain Eq. (8), the Haldane expression should be valid for our finite-SOC SIAM as well, but with band parameters renormalized by SOC (an SOC renormalized parameter will be denoted with a $\tilde{}$ on top of it). Indeed, as illustrated in Fig. 1(d), which compares the DOS for $\gamma = 0.0$ (dotted black line) with that for $|\gamma| = 0.5$ (solid/dashed (red/blue) for $\sigma = \uparrow / \downarrow$), the bulk SOC γ increases the bandwidth and thus decreases the DOS $\tilde{\rho}\left(\epsilon_F\right)$, at $\epsilon_F = 0$. Thanks to the analytical expression for $\epsilon_{k\sigma_r}$ [Eq. (7)], obtained through the spin rotation, we derive simple analytical expressions for the renormalized semi-bandwidth

$$\tilde{D} = 2\sqrt{t^2+|\gamma|^2}, \tag{9}$$

as well as for the band DOS at the Fermi energy $\tilde{\rho}\left(0\right) = 1/\left(2\pi\sqrt{t^2+|\gamma|^2}\right)$. Therefore, the renormalized hybridization function at half filling $\tilde{\Delta} = \tilde{\Delta}\left(0\right)$ can be written as

$$\tilde{\Delta} = \pi\Lambda^2\tilde{\rho}\left(0\right) = \frac{V^2+|\gamma_{imp}|^2}{2\sqrt{t^2+|\gamma|^2}}. \tag{10}$$

Finally, replacing $\tilde{\Delta}$ for Δ in Eq. (8), the renormalized finite-SOC SIAM Kondo temperature $\tilde{T}_K$, in the wide-band limit, is given by

$$\tilde{T}_K = 0.364\left(2\tilde{\Delta}U/\pi\right)^{\frac{1}{2}} \exp\left[\frac{\epsilon_0\left(\epsilon_0+U\right)}{2\tilde{\Delta}U/\pi}\right]. \tag{11}$$

In particular, if one takes the $U \to \infty$ limit, one obtains [1]

$$\tilde{T}_K \propto \sqrt{\tilde{\Delta}\tilde{D}}\exp\left(\pi\epsilon_0/2\tilde{\Delta}\right), \tag{12}$$

where it should be noticed that, differently from the wide-band limit [Eq. (11)], the multiplicative constant in Eq. (12) is unknown. Through the renormalized Haldane expressions given in Eqs. (11) and (12), one can easily analyze the SOC impact on the Kondo temperature. The prefactor in the infinite-U regime depends only on the local SOC term (γ_{imp}) and does not depend on the bulk SOC (γ). However, in the $D \gg U$ regime, the prefactor depends upon both parameters (γ_{imp} and γ). We do not attribute

any specific relevance to this difference in behavior between the two prefactors, as it does not impact the universality of T_K, whose dominant dependence is given by the exponential term shown in Eqs. (11) and (12). In addition (keeping in mind that, in the Kondo regime, $\epsilon_0 < \mu$, since $\epsilon_F = \mu$), Eq. (10), for the renormalized hybridization $\tilde{\Delta}$, implies that the local SOC γ_{imp}, by increasing $\tilde{\Delta}$, exponentially increases $\tilde{T}_K$, while the bulk SOC term γ exponentially decreases it, by decreasing $\tilde{\Delta}$.

Next, we will numerically validate the analytical results obtained for the wide-band regime (using NRG) and for the infinite-U regime (using POA). In addition, we will compare our NRG results with the QMC results in Ref. 15, for the intermediate regime, $U = D > \Delta$, with the Fermi energy close to the bottom of the band.

7. Numerical Results

7.1. Numerical Renormalization Group Results

In Fig. 2, we show Kondo temperature results for finite-SOC, $\tilde{T}_K$ (in $\log_{10}$ scale), as a function of $^U/_{\tilde{\Delta}}$, for $U = 1.0 \times 10^{-3}$, $V = 5.5 \times 10^{-3}$, $0.0 \leq |\gamma| \leq 0.5$, $\gamma_{imp} = 0.0$, $\mu = 0.0$, at the particle-hole symmetric point $\epsilon_0 - \mu = {}^{-U}/_2$. The (red) squares curve was obtained using NRG, while the (blue) circles curve was obtained analytically through Eq. (11). We used this set of parameters for two reasons: first, the wide-band limit, i.e., $D \gg U, \tilde{\Delta}, |\epsilon_0|$, allows for a very precise determination of the prefactor to the exponential [see Eq. (11)]. Thus, in this regime, the Haldane expression is supposed to be the most accurate. This can be confirmed by its very good agreement with NRG, as shown in the figure. Second, for $U \gg \tilde{\Delta}$, and in the particle-hole symmetric point $\epsilon_0 - \mu = {}^{-U}/_2$ and $\mu = 0$, one is deep into the Kondo regime, therefore, NRG is probing the properties of the SIAM very close to its strong coupling fixed point. The very good agreement shown by the results in Fig. 2 imply that the SOC-induced reduction of the Kondo temperature is directly tied to the suppression of the hybridization $\tilde{\Delta}$ at the Fermi energy, which is caused by the widening of the band [see Fig. 1(d)], and this effect is *very accurately* described by the Haldane expression, Eq. (11), giving strong support to the analytical results presented in the previous section.

The situation is more involved for the second regime we analyzed, which we call intermediate regime, i.e., $U = D > \Delta$, where, in addition, we have moved the Fermi energy close to the bottom of the band. Recent results [15], for a model very similar to ours, obtained using QMC, have reported a polynomial dependence of the Kondo temperature with SOC for this intermediate regime (see Fig. 3(a) in Ref. 15). Their conclusion is similar to the one we obtained for the wide-band regime, namely, that the reduction of the hybridization at the Fermi energy, caused by SOC, is responsible for the decrease in the Kondo temperature. In Fig. 3(a), to compare our NRG results with the QMC ones in Ref. 15, it is shown $^{\tilde{T}_K(E_\gamma)}/_{T_K(0)}$ *vs* E_γ [where $E_\gamma = 2[\sqrt{t^2 + |\gamma|^2} - t]$ is the so-called SOC energy, indicated in Fig. 1(b)], for $U = 1.0$, $V = 0.396$, $0.0 \leq |\gamma| \leq 0.5$, $\gamma_{imp} = 0.0$, $\mu = -0.8$, and two different values of $\epsilon_0 - \mu = -0.3$ [(red) squares curve]

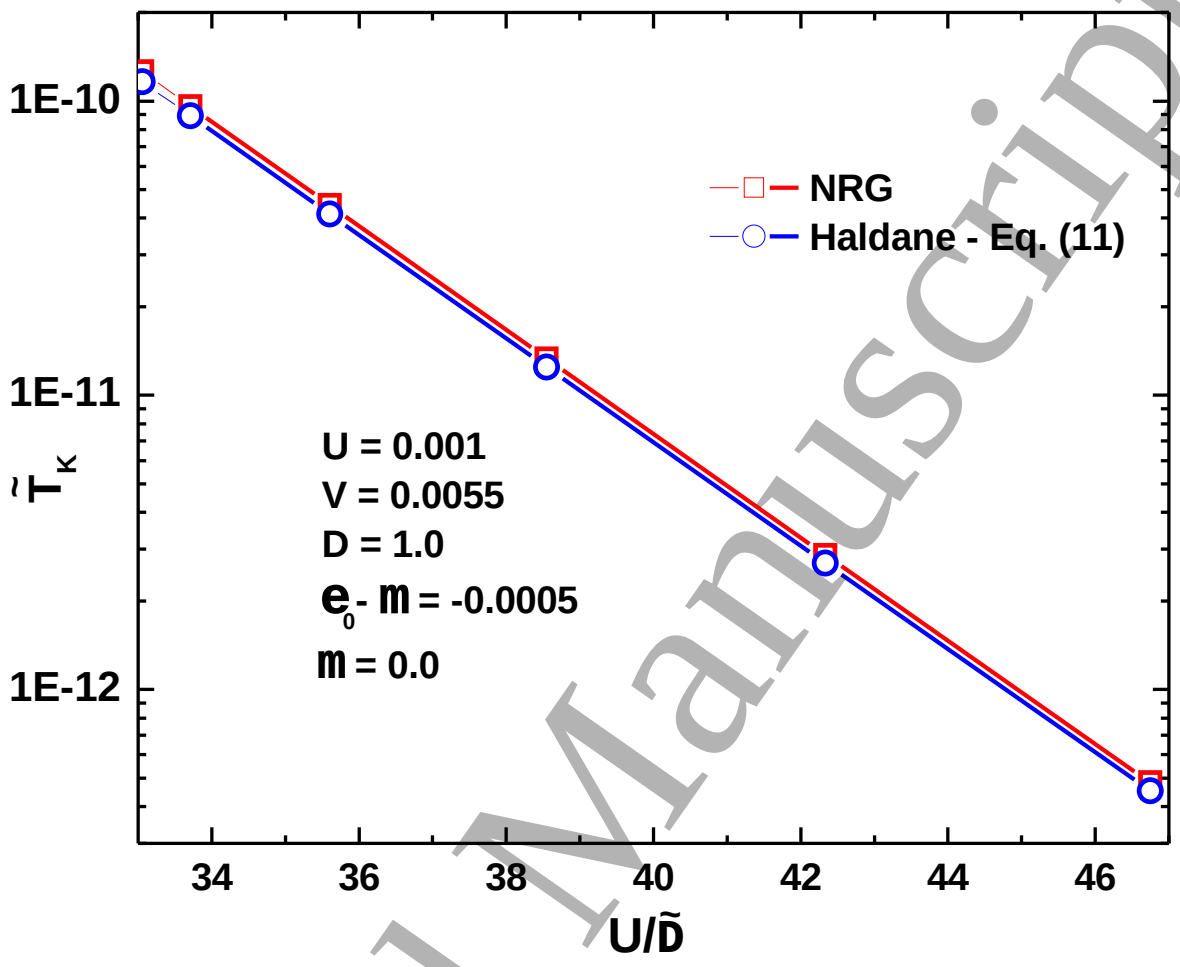

Figure 2. Log-linear plot of $\tilde{T}_K$ *vs* $U/\tilde{\Delta}$, deep into the Kondo regime. Comparison of NRG results [(red) squares curve] with the analytical results obtained from Eq. (11) [(blue) circles curve], for $U = 1.0 \times 10^{-3}$, $V = 5.5 \times 10^{-3}$, $0.0 \leq |\gamma| \leq 0.5$, $\gamma_{imp} = 0.0$, $\mu = 0.0$, and $\epsilon_0 - \mu = -U/2$. The very good agreement indicates that the renormalized Haldane expression [Eq. (11)] describes the dependence of the Kondo temperature with SOC to high accuracy.

and -0.7 [(blue) circles curve]. For this value of chemical potential, the Fermi energy is just 0.2 above the bottom of the band. The contrast to the results shown in Fig. 2 is striking. Note that we have plotted (not shown) the two curves in panel (a) in $\log_{10}$ scale for the vertical axis (*vs* $U/\tilde{\Delta}$) and the behavior is clearly not Haldane-like. In Fig. 3(b), we show NRG results for $\tilde{T}_K(\gamma)/T_K(0)$ *vs* $U/\tilde{\Delta}$ for the same parameters as in Fig. 3(a), but for $\mu = 0.0$ (i.e., at half-filling), using a $\log_{10}$ scale. It is very clear that, *for the particle-hole symmetric point*, contrary to what happens when the Fermi energy is close to the bottom of the band [Fig. 3(b)], $\tilde{T}_K(\gamma)/T_K(0)$, plotted against $U/\tilde{\Delta}$, shows a very-close-to exponential behavior. We do not plot results for the Haldane expression [Eq. (11)] because, as already mentioned above, that expression compares well with the NRG results just for the wide-band limit [35]. Nonetheless, the contrast between the results at half-filling [$\mu = 0.0$, panel (b)] and those for the Fermi energy close to the bottom

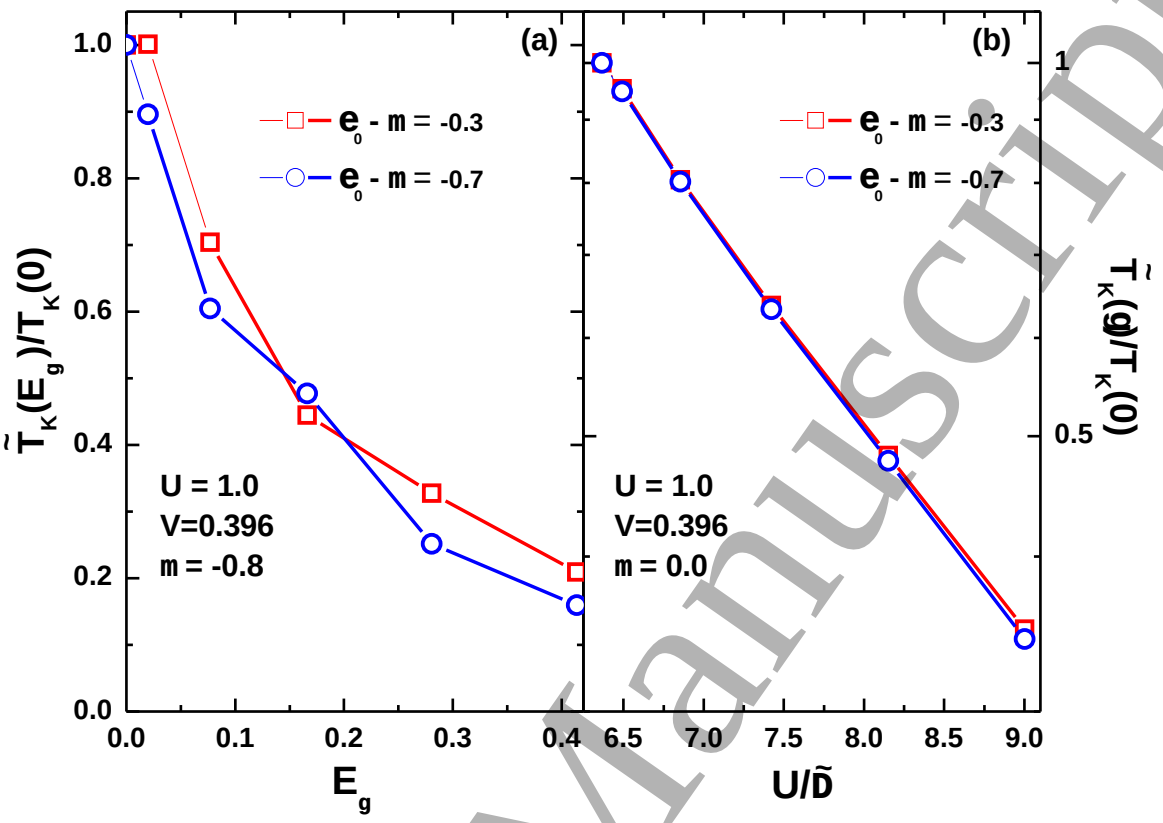

Figure 3. (a) NRG results for $\tilde{T}_K(E_\gamma)/T_K(0)$ *vs* E_γ (SOC energy, see main text) in the intermediate regime, for $U = 1.0$, $V = 0.396$, $0.0 \leq |\gamma| \leq 0.5$, $\gamma_{imp} = 0.0$, $\mu = -0.8$ (thus, the Fermi energy is 0.2 above the bottom of the band), and two different values of $\epsilon_0 - \mu$: -0.3 [(red) squares curve] and -0.7 [(blue) circles curve]. (b) Same parameters as in (a), except for the chemical potential, now at half-filling ($\mu = 0.0$). In addition, the horizontal axis is now $U/\tilde{\Delta}$, instead of E_γ, and the vertical axis is in $\log_{10}$ scale, showing that the Kondo temperature has an almost exponential behavior dependence on $U/\tilde{\Delta}$, similar to the results for the wide-band limit, Fig. 2.

of the band [$\mu = -0.8$, panel (a)], indicates that the polynomial behavior reported in Ref. 15 is caused by the proximity of the Fermi energy, and thus the Kondo peak, to the singularity at the bottom of the band. Indeed, as γ changes, the singularity moves [see Fig. 1(d)], altering its effect over the impurity's local density of states (LDOS), thus over its Kondo peak, and, by extension, over its Kondo temperature. A similar effect was observed for a related 2D model [9, 36]. Indeed, as shown in detail in Ref. 9 [see its Fig. (2)], for $U = D$ and with the Fermi energy sitting close to the bottom of the band, as it is the case for the intermediate regime analyzed here and in Ref. 15, the broad $\epsilon_0 - \mu$ peak in the impurity's LDOS is strongly affected by the singularity at the bottom of the band, and this has an effect on the width of the Kondo peak, thus in the associated Kondo temperature, resulting in the behavior seen in Fig 3(a). None of that is seen in Fig. 2 and very little of it in Fig. 3(b), because both the Kondo and the $\epsilon_0 - \mu$ peaks are far from the singularity and are not affected by its movement (more so in the case of the results in Fig. 2, where, in addition, $U \ll D$). It is not noticeable in

Fig. 3(b), but the first two points ($|\gamma| = 0$ and 0.1), for both values of ϵ_0, slightly deviate from the exponential behavior followed by the rest of the points (at higher $|\gamma|$ values). This is consistent with our interpretation of the non-exponential behavior present for $\mu = -0.8$ being caused by the proximity of the bottom of the band singularity to the Kondo peak, as the singularity moves away from it as SOC increases.

Thus, in summary, the QMC results in Ref. 15, reporting a polynomial behavior of the Kondo temperature with SOC, in qualitative agreement with our results obtained through NRG [see Fig. 3(a)], do not contradict our main conclusion regarding the suitability of using Haldane's expression [Eq. (11)] to understand the SOC effect on the Kondo regime. The reason is clear: the influence of any structures in the hybridization function (like the singularity at its bottom), which only manifests itself in the very specific regime analyzed in Fig. 3(a), where the Fermi energy is close to the bottom of the band and $U = D$, is irrelevant in the wide-band (or flat-band) regime, $\mu = 0.0$ and $D \gg U, \Delta, |\epsilon_0|$, for which Eq. (11) was derived. Finally, we agree with Chen and Han [15] in their assessment that the poor man's scaling results [14], pointing to an exponential increase of T_K with SOC in a 1D system similar to ours, is a high temperature effect, which does not describe the properties of the Kondo ground state under the influence of SOC, at least in regards to the Kondo temperature.

The NRG approach was performed using Wilson's discretization parameter set to $\Lambda = 2.0$, 2000 many-body states were kept after each NRG iteration (except for the calculations near the bottom of the band, where it was necessary to keep 20000), and we made use of the z-trick averaging in the discretization procedure. In addition, the Kondo temperature was obtained through Wilson's criterion [1]. We have used the NRG Ljubljana open source code [37] for all NRG calculations.

7.2. Projector Operator Approach Results

In order to test the analytical results in the infinite-U regime, we use POA, which is a numerical technique that works quite well in this regime [25, 26]. We find the parameter dependence of $\tilde{T}_K$ by calculating the zero-temperature finite-SOC impurity magnetic susceptibility, $\tilde{\chi}_{imp}$. It is obtained by numerically evaluating the impurity magnetization, $M_{imp} = n_{0\uparrow} - n_{0\downarrow}$, due to the application of a vanishing external magnetic field B, coupled just to the impurity and oriented along $\hat{\boldsymbol{r}}$. It is well established that, in the strong coupling regime, $\tilde{\chi}_{imp}(B = 0) = \eta \tilde{T_K}^{-1}$, where η is a constant [1]. Thus, $\tilde{T_K}$ can be obtained (but for a multiplicative constant) through the numerical calculation of $\tilde{\chi}_{imp}$ for a vanishing magnetic field. The objective of these numerical calculations is to confirm Eq. (12).

Figure 4 shows a log-linear plot of $U \to \infty$ POA results for $\tilde{\chi}_{imp}^{-1}/\sqrt{\tilde{\Delta}\tilde{D}}$ *vs* $\epsilon_0/\tilde{\Delta}$, either by varying $-0.17 < \epsilon_0 - \mu < -0.10$ (for $\mu = 0$) and keeping $\tilde{\Delta} = 0.029$ fixed (red squares), or for different values of $\tilde{\Delta}$, obtained by varying $0.10 \leq |\gamma| \leq 0.30$ and $0.23 \leq \Lambda \leq 0.30$, and keeping $\epsilon_0 - \mu = -0.15$ constant (blue triangles). When $\tilde{\Delta}$ and $\tilde{D}$ are varied, an exponential behavior is only obtained after dividing $\tilde{\chi}_{imp}^{-1}$ by $\sqrt{\tilde{\Delta}\tilde{D}}$,

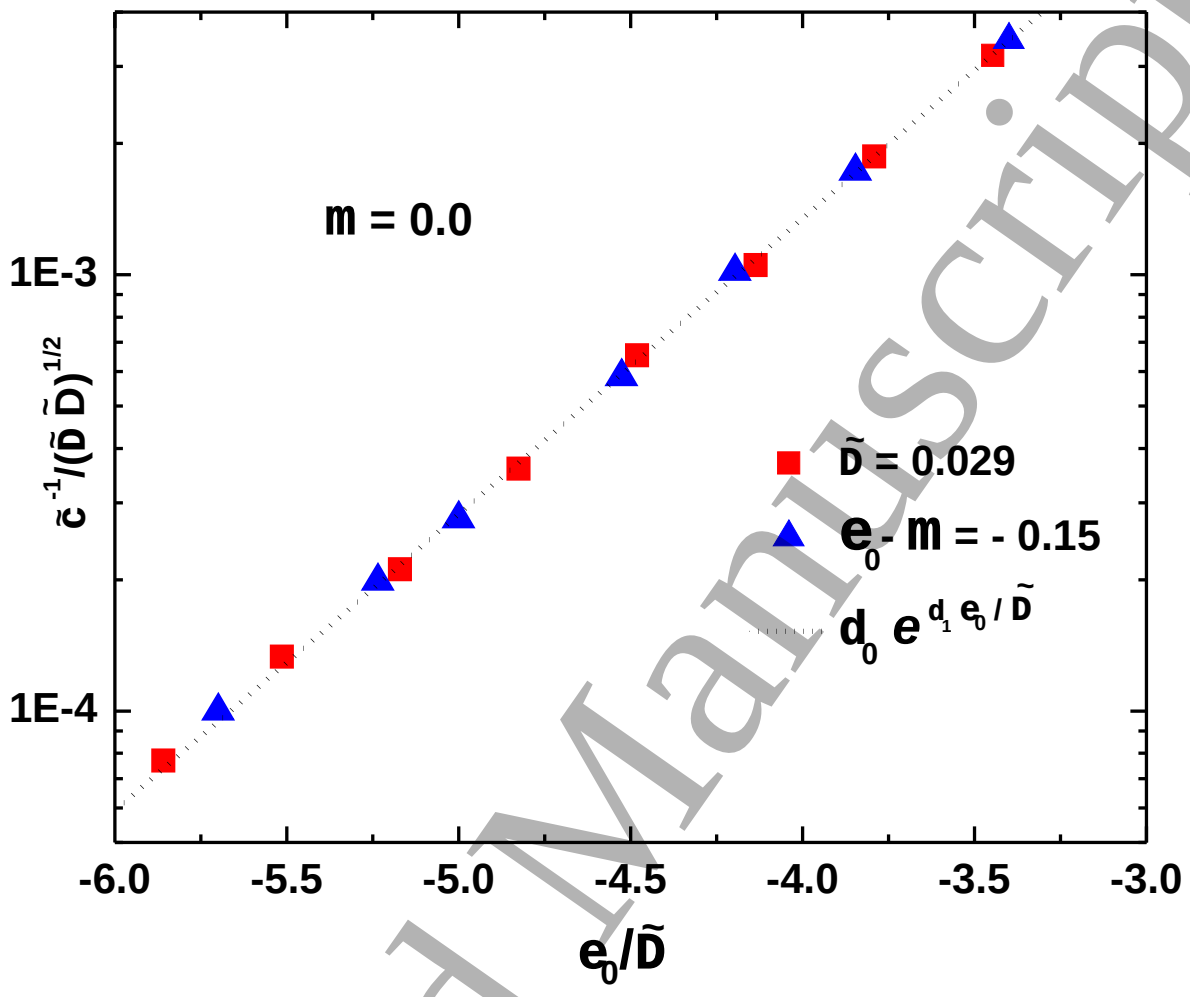

Figure 4. POA results for $\tilde{\chi}_{imp}^{-1}/\sqrt{\tilde{\Delta}\tilde{D}}$ as a function of $\epsilon_0/\tilde{\Delta}$. The (red) squares curve was obtained by varying $-0.17 < \epsilon_0 - \mu < -0.10$, for $\mu = 0$, and keeping $\tilde{\Delta} = 0.029$ fixed, while the (blue) triangles were obtained by varying $\tilde{\Delta}$, by varying simultaneously $0.10 \leq |\gamma| \leq 0.30$ and $0.23 \leq \Lambda \leq 0.30$, and keeping $\epsilon_0 - \mu = -0.15$ constant. The dotted black line is a fitting of the data using $\delta_0 \exp(\delta_1 \epsilon_0/\tilde{\Delta})$, resulting in $\delta_1 = \pi/2$, with $\lesssim 1\%$ error, and $\delta_0 = 0.699$ ($\lesssim 3\%$).

confirming the prefactor dependence shown in Eq. (12). The dotted (black) line is an exponential fit of the data using $\delta_0 \exp(\delta_1 \epsilon_0/\tilde{\Delta})$, resulting in $\delta_1 = \pi/2$ with $\lesssim 1\%$ error, and $\delta_0 = 0.699$ ($\lesssim 3\%$). Therefore, Fig. 4 shows that $\tilde{T}_K$ depends exponentially on $\pi\epsilon_0/2\tilde{\Delta}$, thus corroborating Eq. (12).

8. Summary and conclusions

In conclusion, we have shown, through a physically motivated change of basis, that the 1D finite-SOC SIAM Hamiltonian is similar to that for the zero-SOC SIAM. The form of the 1D finite-SOC SIAM Hamiltonian (for both the S_z and helicity bases) seems to be inappropriate to deal with Kondo physics, since conduction channels with

opposite quantum numbers (either $\sigma = \uparrow\downarrow$ or $\nu = \pm$) are mixed (either by SOC, or by the impurity itself). This issue can be circumvented if one exploits the fact that time-reversal symmetry is not broken. Indeed, it is the time-reversal symmetry that renders the finite-SOC hybridization matrix diagonal and spin-independent (in any spin basis), thus a scalar, like the zero-SOC hybridization function. This can be seen in a more clear way once *both* the impurity and the conduction electrons are rotated to the σ_r basis, where it becomes clear that the spin channels are not mixed neither by SOC, nor by the impurity, allowing a simple analytical treatment of the renormalized $\tilde{T}_K$, through the use of the Haldane expression, which is corroborated by NRG calculations in the wide-band regime ($D \gg U, \Delta, |\epsilon_0|$) and by POA in the infinite-U regime. In addition, NRG results for the intermediate regime ($U = D > \Delta$, with Fermi energy close to the bottom of the band), in qualitative agreement with QMC results presented in Ref. 15, indicate that it is the proximity of the Fermi energy to the structure at the bottom of the hybridization function (a singularity) that causes the divergence of the results from what one expects from Haldane's expression. Finally, it is shown that the 1D SOC-SIAM Hamiltonian, for arbitrary values of α and β, has a PSH SU(2) symmetry, in contrast to the 2D SOC Fermi sea, where the PSH state is restricted to the $\alpha = \beta$ case.

As to a possible experimental verification of our results, we note that it has been demonstrated recently the possibility of controlling the Rashba SOC in InAs nanowires through the use of a combination of metallic gates [38]. InAs nanowires have very strong Rashba SOC, whose strength can be further increased (more than doubled) by the above mentioned technique. The use of a system like that, coupled to either a quantum dot or an adsorbed magnetic impurity could be used to detect the change in T_K caused by the Rashba SOC variation due to the electrostatic fields created by the gates.

The authors hope that the results presented here, as well as the conceptual insights, will be helpful in clarifying the somewhat confusing state of the properties of the Kondo regime of a quantum impurity coupled to a bath subjected to SOC.

Acknowledgments

It is a pleasure to acknowledge discussions with E. Vernek, G.J. Ferreira, and M.S. Figueira. VL acknowledges a PhD scholarship from the Brazilian agency Conselho Nacional de Desenvolvimento Científico e Tecnológico (CNPq), process 160071/2015-1, and financial support from the Generalitat Valenciana through grant reference Prometeo 2017/139. MM acknowledges a PhD scholarship from the Brazilian agency Coordenação de Aperfeiçoamento de Pessoal de Nível Superior (CAPES). GBM acknowledges financial support from CNPq, processes 424711/2018-4 and 305150/2017-0. EVA acknowledges financial support from CNPq, process 306000/2017-2.

References

[1] Hewson A C 1993 *The Kondo Problem to Heavy Fermions* (Cambridge University Press) URL http://dx.doi.org/10.1017/CBO9780511470752

[2] De Haas W J and Van Den Berg G J 1936 *Physica* **3** 440
[3] Kondo J 1964 *Progress of Theoretical Physics* **32** 37 URL http://dx.doi.org/10.1143/PTP.32.37
[4] Meir Y and Wingreen N S 1994 *Phys. Rev. B* **50** 4947
[5] Žutić I, Fabian J and Das Sarma S 2004 *Rev. Mod. Phys.* **76** 323
[6] Bader S and Parkin S 2010 *Annu. Rev. Condens. Matter Phys.* **1** 71
[7] Datta S and Das B 1990 *Applied Physics Letters* **56** 665–667 URL http://dx.doi.org/10.1063/1.102730
[8] Malecki J 2007 *Journal of Statistical Physics* **129** 741–757 ISSN 1572-9613 URL https://doi.org/10.1007/s10955-007-9414-x
[9] Žitko R and Bonča J 2011 *Phys. Rev. B* **84**(19) 193411 URL https://link.aps.org/doi/10.1103/PhysRevB.84.193411
[10] Zarea M, Ulloa S E and Sandler N 2012 *Phys. Rev. Lett.* **108**(4) 046601 URL https://link.aps.org/doi/10.1103/PhysRevLett.108.046601
[11] Mastrogiuseppe D, Wong A, Ingersent K, Ulloa S E and Sandler N 2014 *Phys. Rev. B* **90**(3) 035426 URL https://link.aps.org/doi/10.1103/PhysRevB.90.035426
[12] Wong A, Ulloa S E, Sandler N and Ingersent K 2016 *Phys. Rev. B* **93**(7) 075148 URL https://link.aps.org/doi/10.1103/PhysRevB.93.075148
[13] Chen L, Sun J, Tang H K and Lin H Q 2016 *J. Phys. Condens. Matter* **28** 396005
[14] de Sousa G R, Silva J F and Vernek E 2016 *Phys. Rev. B* **94**(12) 125115 URL https://link.aps.org/doi/10.1103/PhysRevB.94.125115
[15] Chen L and Han R S 2017 *ArXiv e-prints* (*Preprint* 1711.05505)
[16] Gainon D and Heeger A J 1969 *Phys. Rev. Lett.* **22**(26) 1420–1423 URL https://link.aps.org/doi/10.1103/PhysRevLett.22.1420
[17] Wang J and Culcer D 2013 *Phys. Rev. B* **88** 125140
[18] López R, Sánchez D and Serra L 2007 *Phys. Rev. B* **76**(3) 035307 URL https://link.aps.org/doi/10.1103/PhysRevB.76.035307
[19] Haldane F D M 1978 *J. Phys. C: Sol. State Phys.* **11** 5015
[20] Haldane F D M 1978 *Phys. Rev. Lett.* **40** 416 and Phys. Rev. Lett. **40**, 911 (1978)
[21] Bychkov Y A and Rashba E I 1984 *Journal of Physics C: Solid State Physics* **17** 6039 URL http://stacks.iop.org/0022-3719/17/i=33/a=015
[22] Dresselhaus G 1955 *Phys. Rev.* **100**(2) 580–586 URL https://link.aps.org/doi/10.1103/PhysRev.100.580
[23] Winkler R and Zülicke U 2010 *Physics Letters A* **374** 4003
[24] Bernevig B A, Orenstein J and Zhang S C 2006 *Phys. Rev. Lett.* **97** 236601
[25] Roura-Bas P, Hamad I J and Anda E V 2015 *Phys. Status Solidi (b)* **252** 421–430 URL http://dx.doi.org/10.1002/pssb.201451520
[26] Lopes V, Padilla R A, Martins G B and Anda E V 2017 *Phys. Rev. B* **95** 245133
[27] Anderson P W 1961 *Phys. Rev.* **124**(1) 41–53 URL https://link.aps.org/doi/10.1103/PhysRev.124.41
[28] Mireles F and Kirczenow G 2001 *Phys. Rev. B* **64**(2) 024426 URL https://link.aps.org/doi/10.1103/PhysRevB.64.024426
[29] Sun Q f, Wang J and Guo H 2005 *Phys. Rev. B* **71**(16) 165310 URL https://link.aps.org/doi/10.1103/PhysRevB.71.165310
[30] Sakurai J J 1994 *Modern Quantum Mechanics* (Addison-Wesley)
[31] Manchon A, Koo H C, Nitta J, Frolov S M and Duine R A 2015 *Nat. Mater.* **14** 871
[32] Bulla R, Costi T A and Pruschke T 2008 *Rev. Mod. Phys.* **80** 395
[33] Allerdt A, Feiguin A E and Martins G B 2017 *Phys. Rev. B* **96** 035109
[34] Anderson P W 1970 *J. Phys. C: Sol. State Phys.* **3** 2436
[35] It should be noted, as already mentioned at the beginning of Sec. 6, and explained in detail in Sec. 3.4 in Ref. 1, that other approximate analytical expressions for T_K can be obtained for different regimes, but the intermediate regime is not one of them. Note that the three curves in Fig. 3(b) deviate slightly (not shown) from straight lines, most certainly because of a U, $\tilde{\Delta}$, and

$\tilde{D}$ dependent prefactor. In addition, it should be also noted that for none of these expressions a numerical multiplicative factor, like the 0.364 in Eq. (11), has ever been obtained for any regimes other than the wide-band regime [1].

[36] Note that the effect of SOC over the hybridization function in 2D is restricted to the region close to the bottom of the band (see Fig. 4(b) in Ref. 13), while, in 1D, the SOC effect is two-fold: it suppresses the hybridization function at all energies, as well as it moves the singularity at the bottom of the band to lower energies.

[37] R. Žitko, NRG Ljubljana - open source NRG code available at http://nrgljubljana.ijs.si.

[38] Scherübl Z, Fülöp G m H, Madsen M H, Nygård J and Csonka S 2016 *Phys. Rev. B* **94** 035444